Journal of Robotics, Networking and Artificial Life
Vol. 6(1); June (2019), pp. 27–32
DOI: https://doi.org/10.2991/jrnal.k.190531.006; ISSN 2405-9021; eISSN 2352-6386
https://www.atlantis-press.com/journals/jrnal

Research Article

Novel Mathematical Modeling and Motion Analysis of a Sphere Considering Slipping

Kenji Kimura[1,*], Kouki Ogata[2], Kazuo Ishii[1]

[1]Graduate School of Life Science and Engineering, Kyusyu Institute of Technology, 2-4 Hibikino, Wakamatsu-ku, Kitakyushu 808-0196, Fukuoka, Japan
[2]Department of Physics, Faculty of Science and Engineering, Saga University, 1 Honjo, Saga, Saga 840-8421, Japan

ARTICLE INFO

Article History
Received 20 November 2017
Accepted 20 December 2017

Keywords
Angular velocity vector of the sphere
motion analysis of the sphere
slip velocity of the sphere

ABSTRACT

Many mobile robots that use spherical locomotion employ friction-drive systems because such systems offer omnidirectional locomotion and are more capable of climbing steps than omni-wheel systems. One notable issue associated with friction-drive systems is slipping between the sphere and the roller. However, previously established sphere kinematics models do not consider slipping. This study proposes a mathematical model that allows for slipping and can be broadly applied to a variety of mobile robots in a range of situations.

1. INTRODUCTION

Spherical wheels can be used in mobile and omnidirectional robots. For example, the ball wheel [1] comprises a sphere with a circular-roller ring arranged on the outer circumference of the sphere. The propulsive force is generated by the rotation of the oblique-rotation axis. Further, there is no binding force in the direction orthogonal to the propulsion force as there is with an omni-wheel [2]. The omni-ball [3] solves the constraint of the ball wheel [1] as it enables omnidirectional driving via the passive rotation of a pair of hemispheres. It offers similar driving performance as the omni-wheel [2] and superior step-climbing ability.

In mobile robots, Active-Caster [4] is composed of an upper sphere and a lower sphere, each of which is in contact with two driving rollers. The upper sphere uses driving rollers to transmit dynamic motion to the lower sphere. This mechanism is used for driving and steering of the caster and enables omnidirectional motion. The balanced-ball robot [5] achieves omnidirectional locomotion by spherical driving using three omni-wheel arranged on the upper hemisphere of an equilateral triangle. The CPU-ball robot [6] has four-omni-wheel arranged on the upper hemisphere of a regular quadrilateral to achieve spherical driving and realize omnidirectional locomotion.

The RoboCup middle-size-league soccer robot utilizes a ball-dribbling mechanism to control the rotation of the ball. Most of the RoboCup teams, such as the Turtles [7], implemented two constraint rollers on the upper half of the ball. Due to makes strong friction force and enhanced ball-holding ability, most designs use slip-roller arrangements as are determined heuristically via experiments in the absence of suitable mathematical models.

*Corresponding author. Email: kimura_kenji@edu.brain.kyutech.ac.jp

In a previous study, we developed a non-slip omnidirectional-locomotion kinematics model that accounts for the sphere kinematics and roller arrangement [8]. However, this model cannot be used for mobile robots as they also undergo slip locomotion. In this study, we modify the previously developed kinematics model and present a novel mathematical model of sphere rotational motion by two constraint rollers that allows for slipping.

In this paper, the outline of the section is as follows: Section 2 consider discusses the existence space of angular velocity vector and the sphere kinematics by two roller. Section 3 conducted simulation. Finally, we present the summary and discuss future tasks.

2. THE SPHERE KINEMATICS BY CONSTRAINT ROLLERS

In this section, we introduce the angular velocity vector of the sphere to algebraically model the sphere rotational motion.

2.1. The Existence of Angular Velocity Vector of the Sphere by Single-constraint Roller

As shown in Figure 1, the center $\boldsymbol{O}$ of a sphere with radius r is fixed as the origin of the coordinate system $\Sigma - xyz$. Table 1 shows the variables related to the sphere kinematics. The i^{th} constraint roller is in point contact with the sphere at a position vector $\boldsymbol{P}_i$ and is arranged such that the center of mass of the roller $\boldsymbol{P}_i$ and $\boldsymbol{O}$ are on the same line. $\boldsymbol{\omega}$ denotes the angular velocity vector of the sphere. $\boldsymbol{\eta}_i$ denotes the unit vector along the rotational axis of constraint roller.

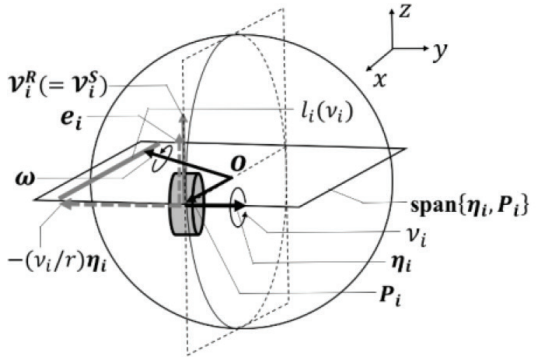

Figure 1 | The existence of sphere angular velocity vector in case of single-constraint roller.

Table 1 | The variables related to the sphere kinematics

Σ–xyz	Three-dimensional coordinate system fixed the sphere
$\langle \boldsymbol{a}, \boldsymbol{b} \rangle$	Inner product with respect to $\boldsymbol{a}$ and $\boldsymbol{b}$
$\|\|\boldsymbol{a}\|\|$	Norm of vector $\boldsymbol{a}$
span{X, Y}	The existence space of $\boldsymbol{\omega}$ allow for slip
$\boldsymbol{O}$	The sphere center
$\boldsymbol{P}_i$	The Position vector of sphere
$\boldsymbol{\eta}_i$	The unit vector along the rotational axis of the constraint-roller
$\boldsymbol{\omega}$	The angular velocity vector of the sphere
$\boldsymbol{\omega}_t$	The orthogonal projection of $\boldsymbol{\omega}$ with respect to **span**{$\boldsymbol{P}_1$, $\boldsymbol{P}_2$}
$\boldsymbol{\omega}_s$	The orthogonal projection of $\boldsymbol{\omega}$ with respect to $\boldsymbol{P}_1 \times \boldsymbol{P}_2$
$\boldsymbol{v}_i^R$	The velocity vector of constraint roller
$\boldsymbol{v}_i^S$	The velocity vector of the sphere
$\boldsymbol{\zeta}_i$	Slip velocity of the sphere with respect to $\boldsymbol{v}_i^R$
$\boldsymbol{e}_i$	The unit normal vector along $\boldsymbol{v}_i^R$
$\boldsymbol{e}$	Upper unit normal vector of **span**{$\boldsymbol{P}_1$, $\boldsymbol{P}_2$}
$\boldsymbol{V}$	Mobile velocity of sphere on xy-plane
{$\boldsymbol{X}_i$, $\boldsymbol{e}$}	Normal orthogonal bases on tangent plane of the sphere at $\boldsymbol{P}_i$
$l_i(v_i)$	Set that exists of end point of $\boldsymbol{\omega}$
$l_i'(v_i)$	The orthogonal projection of $l_i(v_i)$ with respect to **span**{$\boldsymbol{P}_1$, $\boldsymbol{P}_2$}
v_i	Peripheral speed of constraint roller
r	The sphere radius
α_i	The roller arrangement angle between $\boldsymbol{\eta}_i$ and **span**{$\boldsymbol{P}_1$, $\boldsymbol{P}_2$}
φ	Sphere direction
ρ	Angle of sphere rotational axis

v_i denotes the peripheral speed of the constraint roller. Hence, the velocity vector of the sphere $\boldsymbol{v}_i^S$ with respect to $\boldsymbol{P}_i$ can be represented by Equation (1):

$$\boldsymbol{v}_i^S = \boldsymbol{\omega} \times \boldsymbol{P}_i \tag{1}$$

$\boldsymbol{e}_i \in$ **span**{$\boldsymbol{P}_i$, $\boldsymbol{n}_i$} is the unit normal vector along $\boldsymbol{v}_i^R$. Using $v_i = \langle \boldsymbol{v}_i^R, \boldsymbol{e}_i \rangle$ ($\boldsymbol{v}_i^S = \boldsymbol{v}_i^R$: non-slip condition) and Equation (1), v_i is represented as follows:

$$\begin{aligned} v_i &= \langle \boldsymbol{v}_i^R, \boldsymbol{e}_i \rangle = \langle \boldsymbol{\omega} \times \boldsymbol{P}_i, \boldsymbol{e}_i \rangle \\ &= -\langle \boldsymbol{e}_i \times \boldsymbol{P}_i, \boldsymbol{\omega} \rangle = -r \langle \boldsymbol{\eta}_i, \boldsymbol{\omega} \rangle \end{aligned} \tag{2}$$

Thus, $\boldsymbol{\omega}$ can be satisfied as Equation (3).

$$\langle \boldsymbol{\eta}_i, \boldsymbol{\omega} \rangle = -\frac{v_i}{r} \tag{3}$$

Further, from the property of the constraint roller (i.e., that slip does not occur in side direction of the roller), $\boldsymbol{\omega}$ must be on **span**{$\boldsymbol{\eta}_i$, $\boldsymbol{P}_i$}. Thus, Eq. (3) indicates that $\boldsymbol{\omega}$ is constructed as the sum of $(v_i/r)\boldsymbol{\eta}_i$ and $\boldsymbol{P}_i$ (see Figure 1). Thus, $\boldsymbol{\omega}$ cannot be uniquely determined using a single roller. However, the end point set of $\boldsymbol{\omega}$ can be represented as a line set as follows:

$$l_i(v_i) = \left\{ \boldsymbol{\omega} \middle| \left(-\frac{v_i}{r} \right) \boldsymbol{\eta}_i + k\boldsymbol{P}_i,\ k \in \mathbb{R} \right\} \tag{4}$$

2.2. The Existence of Angular Velocity Vector of the Sphere by Two-constraint Rollers

Let the roller arrangement the angle α_i ($-90° \le \alpha_i \le 90°$) between $\boldsymbol{\eta}_i$ and **span**{$\boldsymbol{P}_1$, $\boldsymbol{P}_2$}. Using the normal orthogonal base {$\boldsymbol{X}_i$, $\boldsymbol{e}$} on tangent plane of the sphere at $\boldsymbol{P}_i$, $\boldsymbol{\eta}_i$ can be represented as Equation (5).

$$\boldsymbol{\eta}_i = \boldsymbol{X}_i \cos\alpha_i + \boldsymbol{e} \sin\alpha_i \tag{5}$$

where

$$\boldsymbol{X}_i = r^{-1}\boldsymbol{e} \times \boldsymbol{P}_i,\ \boldsymbol{e} = \frac{\boldsymbol{P}_1 \times \boldsymbol{P}_2}{\|\boldsymbol{P}_1 \times \boldsymbol{P}_2\|} \tag{6}$$

In this section, we consider location between $l_1(v_1)$ and $l_2(v_2)$ which depend on parameter v_1, v_2 (when α_1, α_2 are fixed) and determined the rotational axis of the sphere.

Using Equation (4) (as i = 1, 2), as shown in Figure 2a, if a pair of v_1, v_2 exists such that $l_1(v_1)$ and $l_2(v_2)$ have points in common, the end point of $\boldsymbol{\omega}$ can be uniquely determined. Using Equation (4) (as i = 1, 2), $\boldsymbol{\omega}$ must be on **span**{$\boldsymbol{P}_1$, $\boldsymbol{\eta}_1$}$\cap$**span**{$\boldsymbol{P}_2$, $\boldsymbol{\eta}_2$}. On the other hand, as shown in Figure 2b, if a pair of v_1, v_2 exists such that $l_1(v_1)$ and $l_2(v_2)$ have no points in common, slip can occur.

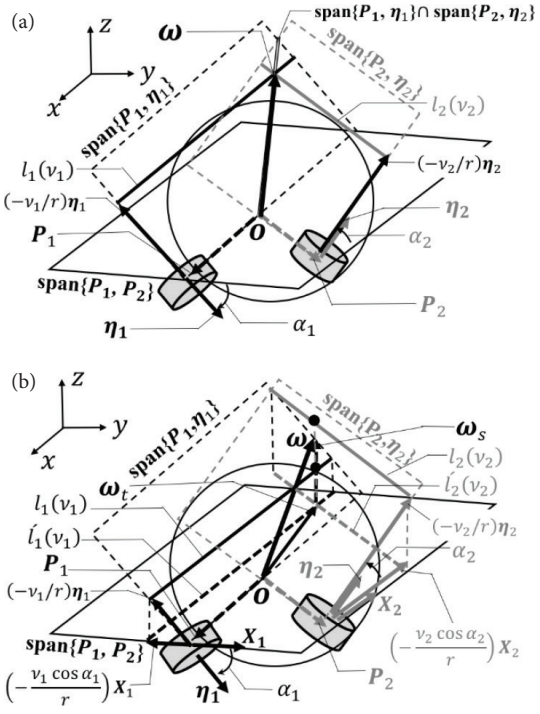

Figure 2 | The location of $l_1(v_1)$ and $l_2(v_2)$. (a) A pair of v_1, v_2 exists such that $l_1(v_1)$ and $l_2(v_2)$ have points in common. (b) A pair of v_1, v_2 exists such that $l_1(v_1)$ and $l_2(v_2)$ have no points in common.

Because the sphere rotational axis is defined with respect to the arbitrary parameters v_1 and v_2, $\boldsymbol{Q}_o \in \mathbb{R}^3$ can be determined such that the sum of the squared distances between $\boldsymbol{Q} \in \mathbb{R}^3$ and $l_i(v_i)$ $(i = 1, 2)$ is minimized. Then, $\boldsymbol{Q}_o$ corresponds to the mid-point between $l_1(v_1)$ and $l_2(v_2)$ [see Appendix (A)]. Using $\boldsymbol{X}_i$, $\boldsymbol{P}_i$, orthogonal projection of $l_i(v_i)$ with respect to $\mathbf{span}\{\boldsymbol{P}_1, \boldsymbol{P}_2\}$ is represented as Equation (7).

$$\acute{l}_i(v_i) = \left\{ \boldsymbol{\omega} \middle| \left(-\frac{v_i \cos\alpha_i}{r} \right) \boldsymbol{X}_i + k\boldsymbol{P}_i, k \in \mathbb{R} \right\} \tag{7}$$

The end point of $\boldsymbol{\omega}_t$ (the orthogonal projection of $\boldsymbol{\omega}$ with respect to $\mathbf{span}\{\boldsymbol{P}_1, \boldsymbol{P}_2\}$) is represented as common point of $\acute{l}_1(v_1)$ and $\acute{l}_2(v_2)$ [see Appendix (B)].

$$\boldsymbol{\omega}_t = \frac{1}{\|\boldsymbol{P}_1 \times \boldsymbol{P}_2\|} \left[(v_2 \cos\alpha_2)\boldsymbol{P}_1 - (v_1 \cos\alpha_1)\boldsymbol{P}_2 \right] \tag{8}$$

A heights $l_i(v_i)$ from $\mathbf{span}\{\boldsymbol{P}_1, \boldsymbol{P}_2\}$ $(i = 1, 2)$, is represented as follows:

$$\frac{-v_1 \sin\alpha_1}{r}, \frac{-v_2 \sin\alpha_2}{r} \tag{9}$$

Using Equation (9), $\boldsymbol{\omega}_s$ (the orthogonal projection of $\boldsymbol{\omega}$ with respect to $\boldsymbol{P}_1 \times \boldsymbol{P}_2$) is represented as mean of these.

$$\boldsymbol{\omega}_s = -\frac{v_1 \sin\alpha_1 + v_2 \sin\alpha_2}{2r} \frac{\boldsymbol{P}_1 \times \boldsymbol{P}_2}{\|\boldsymbol{P}_1 \times \boldsymbol{P}_2\|} \tag{10}$$

Thus, $\boldsymbol{\omega}$ can be represented with respect to v_1 and $v_2 \in \mathbb{R}$.

$$\begin{aligned} \left[\omega_x, \omega_y, \omega_z\right]^T &= \boldsymbol{\omega}_t + \boldsymbol{\omega}_s \\ &= \frac{1}{\|\boldsymbol{P}_1 \times \boldsymbol{P}_2\|} \left[(v_2 \cos\alpha_2)\boldsymbol{P}_1 - (v_1 \cos\alpha_1)\boldsymbol{P}_2 \right] \\ &\quad - \frac{v_1 \sin\alpha_1 + v_2 \sin\alpha_2}{2r} \frac{\boldsymbol{P}_1 \times \boldsymbol{P}_2}{\|\boldsymbol{P}_1 \times \boldsymbol{P}_2\|} \end{aligned} \tag{11}$$

where

$$\boldsymbol{P}_i = r\left[\cos\theta_{1,i} \cos\theta_{2,i}, \sin\theta_{1,i} \cos\theta_{2,i}, \sin\theta_{2,i} \right]^T \tag{12}$$

Specifically, when $\alpha_i = 0°$, the second term of the right-hand side of Equation (11) vanishes. Thus, for all v_1, v_2, $\boldsymbol{\omega} \in \mathbf{span}\{\boldsymbol{P}_1, \boldsymbol{P}_2\}$. In other words, the sphere has omnidirectional locomotion without slip in the expanded form of kinematics model [8].

2.3. The Sphere Kinematics by Two-constraint Rollers

2.3.1. Forward kinematics

φ $(0° \le \varphi < 360°)$ is the angle from x-axis. Mobile velocity of sphere $\boldsymbol{V}$ (the center velocity of sphere) is on xy-plane and represented as Equation (13).

$$\boldsymbol{V} = \|V\| \begin{bmatrix} \cos\varphi & \sin\varphi & 0 \end{bmatrix}^T \tag{13}$$

$\boldsymbol{\omega}$ is perpendicular to $\boldsymbol{V}$, the angle of sphere rotational axis ρ $(-90° \le \rho \le 90°)$ is the angle between $\boldsymbol{\omega}$ and xy-plane. Therefore, using $\boldsymbol{\omega} = [\omega_x, \omega_y, \omega_z]^T$, forward kinematics is given as follows:

$$\begin{aligned} \|V\| &= r\sqrt{\omega_x^2 + \omega_y^2} \\ \varphi &= \begin{cases} \cos^{-1}\left[\dfrac{\omega_y}{\sqrt{\omega_x^2 + \omega_y^2}} \right] (\omega_x < 0) \\ 360° - \cos^{-1}\left[\dfrac{\omega_y}{\sqrt{\omega_x^2 + \omega_y^2}} \right] (\omega_x \ge 0) \end{cases} \\ \rho &= \tan^{-1}\left[\frac{\omega_z}{\sqrt{\omega_x^2 + \omega_y^2}} \right] \end{aligned} \tag{14}$$

2.3.2 Inverse kinematics

From Equations (13) and (14), $\boldsymbol{\omega}$ is represented as Equation (15).

$$\left[\omega_x, \omega_y, \omega_z\right]^T = \frac{\|V\|}{r} \left[-\sin\varphi, \cos\varphi, \tan\rho \right]^T \tag{15}$$

By rearranging Equation (11), following equation can be obtained as linear combination of $\boldsymbol{X}$ and $\boldsymbol{Y}$.

$$\boldsymbol{\omega} = v_2 \boldsymbol{X} + v_1 \boldsymbol{Y} \tag{16}$$

where

$$\begin{aligned} \boldsymbol{X} &= \frac{\cos\alpha_2}{\|\boldsymbol{P}_1 \times \boldsymbol{P}_2\|} \boldsymbol{P}_1 - \frac{\sin\alpha_2}{2r} \frac{\boldsymbol{P}_1 \times \boldsymbol{P}_2}{\|\boldsymbol{P}_1 \times \boldsymbol{P}_2\|} \\ \boldsymbol{Y} &= -\frac{\cos\alpha_1}{\|\boldsymbol{P}_1 \times \boldsymbol{P}_2\|} \boldsymbol{P}_2 - \frac{\sin\alpha_1}{2r} \frac{\boldsymbol{P}_1 \times \boldsymbol{P}_2}{\|\boldsymbol{P}_1 \times \boldsymbol{P}_2\|} \end{aligned} \tag{17}$$

Thus, for all v_1, v_2, $\mathbf{span}\{\boldsymbol{X}, \boldsymbol{Y}\}$ is two-dimensional-freedom existence space, which has the unit vector $\boldsymbol{X} \times \boldsymbol{Y}$. From $\boldsymbol{\omega} \in \mathbf{span}\{\boldsymbol{X}, \boldsymbol{Y}\}$, using Equation (15) and $\langle \boldsymbol{\omega}, \boldsymbol{X} \times \boldsymbol{Y} \rangle = 0$, ρ is obtained as follows:

$$\rho = \tan^{-1}\left[\frac{(\boldsymbol{X} \times \boldsymbol{Y})_x \sin\varphi - (\boldsymbol{X} \times \boldsymbol{Y})_y \cos\varphi}{(\boldsymbol{X} \times \boldsymbol{Y})_z} \right] \tag{18}$$

where $(\boldsymbol{X} \times \boldsymbol{Y})_x$, $(\boldsymbol{X} \times \boldsymbol{Y})_y$ and $(\boldsymbol{X} \times \boldsymbol{Y})_z$ are components of $\boldsymbol{X} \times \boldsymbol{Y}$.

When Equation (18) is substituted in Equation (15), $\boldsymbol{\omega}$ is obtained as follows:

$$\begin{aligned} &\left[\omega_x, \omega_y, \omega_z\right]^T = \\ &\frac{\|V\|}{r} \left[-\sin\varphi, \cos\varphi, \frac{(\boldsymbol{X} \times \boldsymbol{Y})_x \sin\varphi - (\boldsymbol{X} \times \boldsymbol{Y})_y \cos\varphi}{(\boldsymbol{X} \times \boldsymbol{Y})_z} \right]^T \end{aligned} \tag{19}$$

And, from Equation (7), $\boldsymbol{\omega}$ is satisfied as

$$\langle \boldsymbol{\omega}, \boldsymbol{X}_i \rangle = -\frac{v_i \cos\alpha_i}{r} \tag{20}$$

Using Equation (6), $\langle \boldsymbol{\omega}, \boldsymbol{X}_i \rangle$ is calculated as follows:

$$\begin{aligned} \langle \boldsymbol{\omega}, \boldsymbol{X}_i \rangle &= r^{-1} \langle \boldsymbol{\omega}, \boldsymbol{e} \times \boldsymbol{P}_i \rangle \\ &= -r^{-1} \langle \boldsymbol{e}, \boldsymbol{\omega} \times \boldsymbol{P}_i \rangle \end{aligned} \tag{21}$$

Thus, from Equations (20) and (21), v_i is obtained as follows:

$$v_i = \frac{\langle \boldsymbol{e}, \boldsymbol{\omega} \times \boldsymbol{P}_i \rangle}{\cos\alpha_i} \tag{22}$$

2.4. Slip Velocity of the Sphere

Slip occurs when the roller velocity $\boldsymbol{v}_i^R$ and the sphere velocity $\boldsymbol{v}_i^S$ on the tangent plane **span**$\{\boldsymbol{X}_i, \boldsymbol{e}\}$ at the point $\boldsymbol{P}_i$ are different. Slip velocity of sphere $\boldsymbol{\zeta}_i$ which is relative speed with respect to $\boldsymbol{v}_i^R$ can be represented as difference between $\boldsymbol{v}_i^S$ and $\boldsymbol{v}_i^R$ as Equation (23).

$$\boldsymbol{\zeta}_i = \boldsymbol{v}_i^S - \boldsymbol{v}_i^R \tag{23}$$

where

$$\boldsymbol{v}_i^S = \boldsymbol{\omega} \times \boldsymbol{P}_i, \boldsymbol{v}_i^R = v_i \boldsymbol{e}_i \tag{24}$$

Here, we substitute (24) for $\boldsymbol{v}_i^S$ and $\boldsymbol{v}_i^R$ in Equation (23).

$$\boldsymbol{\zeta}_i = \boldsymbol{\omega} \times \boldsymbol{P}_i - v_i \boldsymbol{e}_i \tag{25}$$

Taking the inner product with $\boldsymbol{e}$ on both sides of Equation (25) and using Equation (22) in the first term on the right-side and Equation (5) in the second term of the right-side, the following Equation (26) can be formulated.

$$\langle \boldsymbol{\zeta}_i, \boldsymbol{e} \rangle = \langle \boldsymbol{\omega} \times \boldsymbol{P}_i, \boldsymbol{e} \rangle + v_i \langle \boldsymbol{e}_i, \boldsymbol{e} \rangle = v_i \cos\alpha_i - v_i \cos\alpha_i = 0 \tag{26}$$

Thus, $\boldsymbol{\zeta}_i$ is parallel to $\boldsymbol{X}_i$ ($\boldsymbol{e}$-component vanished) and represented as

$$\boldsymbol{\zeta}_i = S_i \boldsymbol{X}_i \tag{27}$$

where

$$S_i = \langle \boldsymbol{\zeta}_i, \boldsymbol{X}_i \rangle \tag{28}$$

3. SIMULATION

This section presents the simulation results, including the trajectory of the end point of the angular velocity vector, the angle of the sphere rotational axis, the peripheral speed of the constraint roller, and $\boldsymbol{X}_i$-component of the slip velocity in the given mobile speed of the sphere: $||V||$=1 m/s. The conditions are as follows: r = 1 (m), $\theta_{1,1}$ = 215°, $\theta_{1,2}$ = 325°, $\theta_{1,2}$, $\theta_{2,2}$ = 60°, and $\alpha_2 = -\alpha_1$. Simulations were conducted at the four different angles, α_1 [represented as k; curve color]. Further, $\boldsymbol{\omega}_k$, ρ_k, $v_{i,k}$, and $S_{i,k}$ (k = 0, 1, 2, 3) were indicated such as α_i = 0° [k = 0; red curve], α_i = 10° [k = 1; blue curve], α_i = 20° [k = 2; green curve], and α_i = 30° [k = 3; pink curve]. They are calculated from Equations (18), (19), (22), and (28), respectively. As shown in Figure 3a, ellipsoid trajectories $\boldsymbol{\omega}_k$ (k = 0, 1, 2, 3) are getting scarp in turn and have a common line parallel to the x-axis.

As shown in Figure 3b, ρ_k (k = 0, 1, 2, 3) satisfy the inequality $|\rho_0| < |\rho_1| < |\rho_2| < |\rho_3|$ for all φ. Specifically, when φ = 90° or 270°, ρ_k = 0°. Thus, the sphere undergoes pure rotation (forward and backward movement).

As shown in Figure 3c, $v_{i,k}$ (k = 0, 1, 2, 3) are satisfied $|v_{i,0}| < |v_{i,1}| < |v_{i,2}| < |v_{i,3}|$ (i = 1, 2) For all φ. Specifically, where φ = 0° and 180° (right and left side forward movement), $v_{1,k} = -v_{2,k}$ (opposite sign). Where φ = 90° and 270°, $v_{1,k} = v_{2,k}$ and $|v_{i,0}|$ = 0.91, $|v_{i,1}|$ = 0.93, $|v_{i,2}|$ = 0.96, $|v_{i,3}|$ = 1.03 (m/s).

As shown in Figure 3d, $S_{i,k}$ (k = 0, 1, 2, 3) satisfy the inequality $|S_{i,0}| < |S_{i,1}| < |S_{i,2}| < |S_{i,3}|$ (i = 1, 2) for all φ. From Equation (26), where 0° < φ < 180°, $\boldsymbol{\zeta}_{1,k}$ and $\boldsymbol{\zeta}_{2,k}$ are face-to-face. In contrast, where 180° < φ < 360°, $\boldsymbol{\zeta}_{1,k}$ and $\boldsymbol{\zeta}_{2,k}$ are back-to-back. Specifically, when φ = 0° and 180°, the sphere slip speed is $||\boldsymbol{\zeta}_{1,k}|| = ||\boldsymbol{\zeta}_{2,k}|| = 0$ m/s. Specifically, when φ = 90° and 270°, $|S_{1,k}|$ and $|S_{2,k}|$ are at their maxima ($|S_{1,0}| = |S_{2,0}| = 0$, $|S_{1,1}| = |S_{2,1}| = 0.16$, $|S_{1,2}| = |S_{2,2}| = 0.32$, and $|S_{1,3}| = |S_{2,3}| = 0.52$ m/s).

Further, when α_1 = 0°, $|S_{1,0}| = |S_{2,0}| = 0$ for all φ. Thus, in this case, the sphere has omnidirectional locomotion without slip. Moreover, the proposed model includes the previously developed model [8].

4. CONCLUSION

Herein, we consider the existence of an angular velocity vector for the sphere and propose a sphere kinematics model that allows

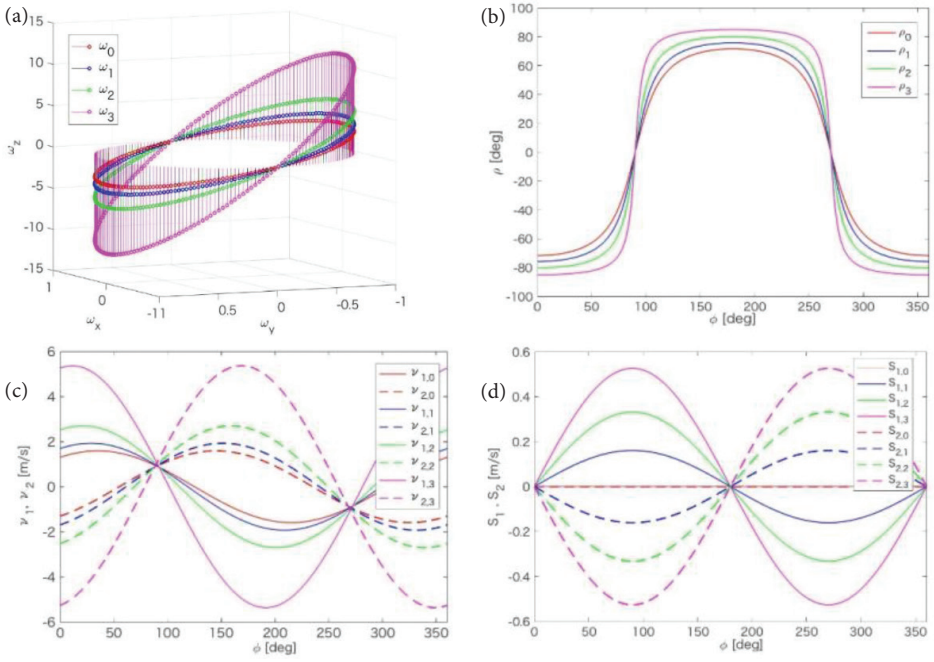

Figure 3 | Comparison in case of α_1 = 0°, 10°, 20°, 30° in simulation. (a) Trajectory of end point of angular velocity vector of the sphere. (b) Angle of the sphere rotational axis. (c) Rollers peripheral speed. (d) $\boldsymbol{X}_i$-component of slip velocity of the sphere.

for slipping. In addition, we demonstrate the trajectory of the end point of the angular velocity vectors of the roller speed and slip speed of the sphere in simulations. This model includes the previously developed model [8] and is expected to be applicable to a wide range of mobile robots in a variety of situations.

In future studies, this model should be verified experimentally. Further, it could be applied to simulate the ball-dribbling mechanism.

CONFLICTS OF INTEREST

There is no conflicts of interest.

APPENDIX (A) CALCULATION OF MINIMAL POINT Q_0

As shown in Figure 4a, d_i denote the distance between $\boldsymbol{Q} \in \mathbb{R}^3$ and line l_i (i = 1, 2). $\boldsymbol{Q}_i$ denote the points at which a perpendicular line intersects l_i (i = 1, 2). Using follow

Lemma. Let k_0 be the minimum value of $d_1 + d_2$ and $M_k = \{\boldsymbol{X} | d_1 + d_2 = k, k_0 \le k, k \in \mathbb{R}, \boldsymbol{X} \in \mathbb{R}^3\}$.

The following statements hold:

(i) $k \neq \acute{k} \Leftrightarrow M_k \cap M_{\acute{k}} = \phi$

(ii) $\cup_{k_0 \le k} M_k = \mathbb{R}^3$

Problem (A): Minimum of $d_1^2 + d_2^2$ such that $(x, y, z) \in \mathbb{R}^3$ is equivalent to Problem (B): Minimum of $d_1^2 + d_2^2$ such that $(d_1, d_2) \in \{(d_1, d_2) | k_0 \le d_1 + d_2, 0 \le d_1, d_2\}$.

Thus, as shown in Figure 4b, when the line defined by $d_1 + d_2 = k_0$ is tangent to the circle defined by $d_1^2 + d_2^2 = k/2$ at $(d_1, d_2) = (k_0/2, k_0/2)$, $d_1^2 + d_1^2$ is minimized. Thus, $\boldsymbol{Q}_0 \in \mathbb{R}^3$ is the midpoint of l_1 and l_2.

APPENDIX (B) CALCULATION OF ω_t

As shown in Figure 5, following expressions are completed.

$$\angle \boldsymbol{X}_1\boldsymbol{O}\boldsymbol{P}_2 = \angle \boldsymbol{P}_1\boldsymbol{O}\boldsymbol{P}_2 - 90^\circ \tag{B.1}$$

$$\angle \boldsymbol{X}_2\boldsymbol{O}\boldsymbol{P}_1 = 180^\circ - \angle \boldsymbol{X}_1\boldsymbol{O}\boldsymbol{P}_2 \tag{B.2}$$

and,

$$\sin \angle \boldsymbol{P}_1\boldsymbol{O}\boldsymbol{P}_2 = r^{-2} \| \boldsymbol{P}_1 \times \boldsymbol{P}_2 \| \tag{B.3}$$

Using Equations (B.1) and (B.3), $\langle \boldsymbol{P}_2, \boldsymbol{X}_1 \rangle$ are represented as Equation (B.4).

$$\begin{aligned} \langle \boldsymbol{P}_2, \boldsymbol{X}_1 \rangle &= \|\boldsymbol{P}_2\| \|\boldsymbol{X}_1\| \cos(\angle \boldsymbol{P}_1\boldsymbol{O}\boldsymbol{P}_2 - 90^\circ) \\ &= r \sin(\angle \boldsymbol{P}_1\boldsymbol{O}\boldsymbol{P}_2) = r^{-1} \|\boldsymbol{P}_1 \times \boldsymbol{P}_2\| \end{aligned} \tag{B.4}$$

Using Equations (B.2) and (B.4), $\langle \boldsymbol{P}_1, \boldsymbol{X}_2 \rangle$ are represented as Equation (B.5).

$$\langle \boldsymbol{P}_1, \boldsymbol{X}_2 \rangle = -\langle \boldsymbol{P}_2, \boldsymbol{X}_1 \rangle = -r^{-1} \|\boldsymbol{P}_1 \times \boldsymbol{P}_2\| \tag{B.5}$$

$\boldsymbol{\omega}_t$ can be represented as shown in Equation (B.6).

$$\boldsymbol{\omega}_t = (C_1\boldsymbol{P}_1 + C_2\boldsymbol{P}_2), C_1, C_1 \in \mathbb{R} \tag{B.6}$$

In both the sides of Equation (B.6), taking inner product with respect to $\boldsymbol{X}_i$. $\langle \boldsymbol{\omega}_t, \boldsymbol{X}_i \rangle$ is represented as Equation (B.7).

$$\langle \boldsymbol{\omega}_t, \boldsymbol{X}_i \rangle = C_1 \langle \boldsymbol{P}_1, \boldsymbol{X}_i \rangle + C_2 \langle \boldsymbol{P}_2, \boldsymbol{X}_i \rangle \tag{B.7}$$

Using Equation (20), $\boldsymbol{\omega}_t$ is satisfied Equation (B.8).

$$\langle \boldsymbol{\omega}_t, \boldsymbol{X}_i \rangle = -\frac{v_i \cos \alpha_i}{r} \tag{B.8}$$

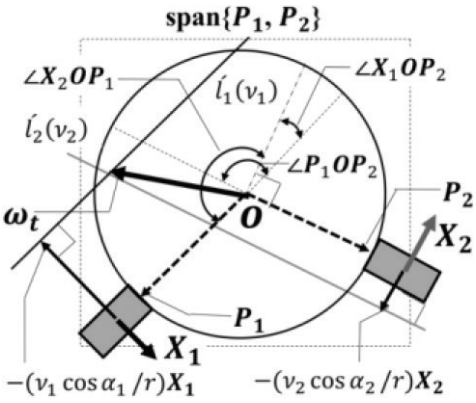

Figure 5 | The end point of ω_t on **span**$\{\boldsymbol{P}_1, \boldsymbol{P}_2\}$ is determine as common point $\acute{l}_1(v_1)$ and $\acute{l}_2(v_2)$.

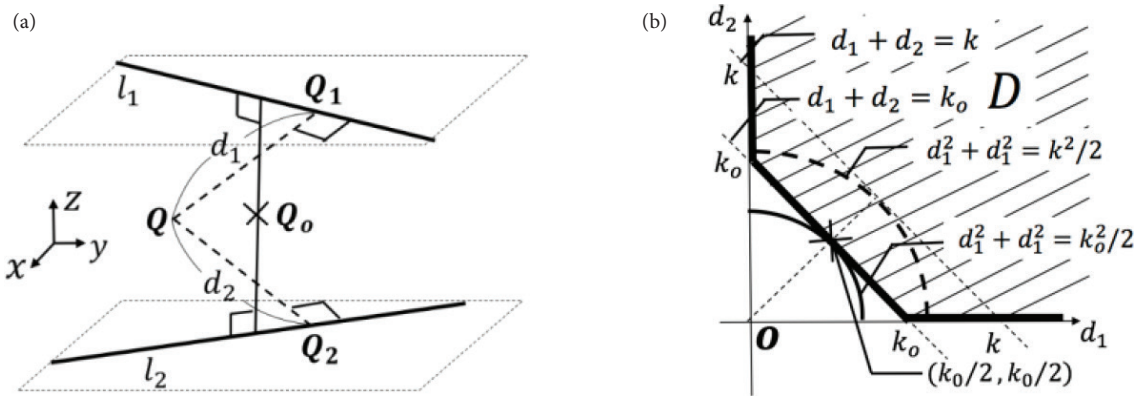

Figure 4 | Minimum problem of sum of squares distance. (a) Problem (A): Minimum $d_1^2 + d_2^2$ such that $(x, y, z) \in \mathbb{R}^3$. (b) Problem (B): Minimum $d_1^2 + d_2^2$ such that $(d_1, d_2) \in \boldsymbol{D}$.

Using $\langle \boldsymbol{P}_i, \boldsymbol{X}_i \rangle = 0$ and Equation (B.8), right side of Equation (B.7) is represented as Equation (B.9).

$$-\frac{v_2 \cos\alpha_2}{r} = C_1 \langle \boldsymbol{P}_1, \boldsymbol{X}_2 \rangle, -\frac{v_1 \cos\alpha_1}{r} = C_2 \langle \boldsymbol{P}_2, \boldsymbol{X}_1 \rangle \tag{B.9}$$

Thus, using Equation (B.5), C_1 and C_2 are represented as Equation (B.10).

$$C_1 = \frac{v_2 \cos\alpha_2}{\|\boldsymbol{P}_1 \times \boldsymbol{P}_2\|}, \; C_2 = \frac{-v_1 \cos\alpha_1}{\|\boldsymbol{P}_1 \times \boldsymbol{P}_2\|} \tag{B.10}$$

Equation (B.10) is substituted in Equation (B.6). Thus, it is given.

REFERENCES

[1] M. West, H. Asada, Design of a holonomic omnidirectional vehicle, Proceedings of the 1992 IEEE International Conference on Robotics and Automation, IEEE, Nice, France, France, 1992, pp. 97–103.

[2] K. Tadakuma, R. Tadakuma, J. Berengeres, Development of holonomic omnidirectional vehicle with "Omni-Ball": spherical wheels, 2007 IEEE/RSJ International Conference on Intelligent Robots and Systems, IEEE, San Diego, CA, USA, 2007, pp. 33–39.

[3] S. Fujisawa, K. Ohkubo, Y. Shidama, H. Yamaura, Kinematics and traveling characteristics of four-wheel independent drive type omnidirectional mobile robot, Trans. JSME 62 (1996), 4573–4579.

[4] M. Wada, Y. Inoue, T. Hirama, Kinematics and mechanical design of an active-caster with a ball transmission, J. Robot. Soc. Japan 31 (2013), 591–598.

[5] M. Kumaga, T. Ochiai, Development of a robot balanced on a ball — Application of passive motion to transport —, 2009 IEEE International Conference on Robotics and Automation, IEEE, Kobe, Japan, 2009, pp. 4106–4111.

[6] T. Endo, Y. Nakamura, An omnidirectional vehicle on a basketball, ICAR '05. Proceedings., 12th International Conference on Advanced Robotics, 2005, IEEE, Seattle, WA, USA, 2005, pp. 573–578.

[7] W. Houtman, Design of a ball clamping system for robocup middle size league robots, Bachelor Final Project, Eindhoven University, 2014, pp. 9–20.

[8] K. Kimura, K. Ishii, Y. Takemura, M. Yamamoto, Mathematical modeling and motion analysis of the wheel based ball retaining mechanism, 2016 Joint 8th International Conference on Soft Computing and Intelligent Systems (SCIS) and 17th International Symposium on Advanced Intelligent Systems (ISIS), IEEE, Sapporo, Japan, 2016, pp. 518–523.

Authors Introduction

Mr. Kenji Kimura

He received the M.E. (mathematics) from Kyusyu University in 2002. Then he was a mathematical teacher and involved in career guidance in high school up to 2014. He currently, is instructor of International Baccalaureate Diploma Program (Mathematics: applications and interpretation, analysis and approaches) in Fukuoka Daiichi High School, and student in the doctoral program of the Kyushu Institute of Technology. His current research interest spherical mobile robot kinematics, control for object manipulation, and human body motion Bernsteinns degrees-of freedom problem.

Dr. Kazuo Ishii

He is a Professor in the Kyushu Institute of Technology, where he has been since 1996. He received his PhD degree in engineering from University of Tokyo, Tokyo, Japan, in 1996. His research interests span both ship marine engineering and Intelligent Mechanics. He holds five patents derived from his research. His lab got "Robo Cup 2011 Middle Size League Technical Challenge 1st Place" in 2011. He is a member of the Institute of Electrical and Electronics Engineers, the Japan Society of Mechanical Engineers, Robotics Society of Japan, the Society of Instrument and Control Engineers and so on.

Mr. Kouki Ogata

He received high school diploma in Fukuoka Daiichi high school until 2016. He is currently under Graduate School student at Saga University. His current research interest sphere mobile robot kinematics, control, analytical dynamics.